Draft version May 7, 2021
Typeset using LaTeX **preprint** style in AASTeX63

Search for Solar Flare Neutrinos with the KamLAND detector

S. Abe,[1] S. Asami,[1] A. Gando,[1] Y. Gando,[1] T. Gima,[1] A. Goto,[1] T. Hachiya,[1] K. Hata,[1] S. Hayashida,[1,*] K. Hosokawa,[1] K. Ichimura,[1] S. Ieki,[1] H. Ikeda,[1] K. Inoue,[1,2] K. Ishidoshiro,[1] Y. Kamei,[1] N. Kawada,[1] Y. Kishimoto,[1,2] T. Kinoshita,[1] M. Koga,[1,2] N. Maemura,[1] T. Mitsui,[1] H. Miyake,[1] K. Nakamura,[1] K. Nakamura,[1] R. Nakamura,[1] H. Ozaki,[1,3] T. Sakai,[1] H. Sambonsugi,[1] I. Shimizu,[1] J. Shirai,[1] K. Shiraishi,[1] A. Suzuki,[1] Y. Suzuki,[1] A. Takeuchi,[1] K. Tamae,[1] K. Ueshima,[1,†] Y. Wada,[1] H. Watanabe,[1] Y. Yoshida,[1] S. Obara,[4] A. Kozlov,[2,‡] D. Chernyak,[2,§] Y. Takemoto,[5,¶] S. Yoshida,[5] S. Umehara,[6] K. Fushimi,[7] A. K. Ichikawa,[8,9] K. Z. Nakamura,[8] M. Yoshida,[8] B. E. Berger,[10,2] B. K. Fujikawa,[10,2] J. G. Learned,[11] J. Maricic,[11] S. N. Axani,[12] L. A. Winslow,[12] Z. Fu,[12] J. Ouellet,[12] Y. Efremenko,[13,2] H. J. Karwowski,[14,15] D. M. Markoff,[14,16] W. Tornow,[14,17,2] A. Li,[15] J. A. Detwiler,[18,2] S. Enomoto,[18,2] M. P. Decowski,[19,2] C. Grant,[20] T. O'Donnell,[21] S. Dell'Oro,[21]

(KamLAND Collaboration)

[1] *Research Center for Neutrino Science, Tohoku University, Sendai 980-8578, Japan*
[2] *Institute for the Physics and Mathematics of the Universe, The University of Tokyo, Kashiwa 277-8568, Japan*
[3] *Graduate Program on Physics for the Universe, Tohoku University, Sendai 980-8578, Japan*
[4] *Frontier Research Institute for Interdisciplinary Sciences, Tohoku University, Sendai, 980-8578, Japan*
[5] *Graduate School of Science, Osaka University, Toyonaka, Osaka 560-0043, Japan*
[6] *Research Center for Nuclear Physics (RCNP), Osaka University, Ibaraki, Osaka 567-0047, Japan*
[7] *Graduate School of Advanced Technology and Science, Tokushima University, Tokushima, 770-8506, Japan*
[8] *Department of Physics, Kyoto University, Kyoto 606-8502, Japan*
[9] *Department of Physics, Tohoku University, Sendai 980-8578, Japan*
[10] *Nuclear Science Division, Lawrence Berkeley National Laboratory, Berkeley, CA 94720, USA*
[11] *Department of Physics and Astronomy, University of Hawaii at Manoa, Honolulu, HI 96822, USA*
[12] *Massachusetts Institute of Technology, Cambridge, MA 02139, USA*
[13] *Department of Physics and Astronomy, University of Tennessee, Knoxville, TN 37996, USA*
[14] *Triangle Universities Nuclear Laboratory, Durham, NC 27708, USA*
[15] *The University of North Carolina at Chapel Hill, Chapel Hill, NC 27599, USA*
[16] *North Carolina Central University, Durham, NC 27701, USA*
[17] *Physics Department at Duke University, Durham, NC 27705, USA*
[18] *Center for Experimental Nuclear Physics and Astrophysics, University of Washington, Seattle, WA 98195, USA*
[19] *Nikhef and the University of Amsterdam, Science Park, Amsterdam, The Netherlands*
[20] *Boston University, Boston, MA 02215, USA*
[21] *Center for Neutrino Physics, Virginia Polytechnic Institute and State University, Blacksburg, VA 24061, USA*

(Received May 6, 2021; Revised MM dd, yyyy; Accepted MM dd, yyyy)

Submitted to ApJ

Corresponding author: N. Kawada
kawada@awa.tohoku.ac.jp

ABSTRACT

We report the result of a search for neutrinos in coincidence with solar flares from the *GOES* flare database. The search was performed on a 10.8 kton-year exposure of KamLAND collected from 2002 to 2019. We found no statistical excess of neutrinos and established 90% confidence level upper limits of $8.4 \times 10^7\,\mathrm{cm}^{-2}$ ($3.0 \times 10^9\,\mathrm{cm}^{-2}$) on electron anti-neutrino (electron neutrino) fluence at 20 MeV normalized to the X12 flare, assuming that the neutrino fluence is proportional to the X-ray intensity. The 90% C.L. upper limits from this work exclude the entire region of parameter space associated with the Homestake event excess for the large solar flare in 1991.

Keywords: neutrinos — Sun: flares

1. INTRODUCTION

Solar flares are the largest explosions in the solar system, releasing energy between 10^{28}–10^{33} erg in only tens of minutes (Schrijver et al. 2012). The mechanism of solar flares can be described as a rapid conversion of magnetic energy to thermal and kinetic energy of charged particles by reconnection of the magnetic field on the solar surface (Shibata 1998). Observations of electromagnetic signals, ranging from radio waves to γ-rays at 100 MeV, and neutrons emitted during solar flares contribute to the current understanding of this phenomenon (Benz 2008).

In the standard flare model, solar flares accelerate protons up to about 200 GeV and then nuclear reactions of accelerated protons generate pions in the solar atmosphere. Decay of these pions produce high energy (>50 MeV) γ-rays and neutrinos. Thus, neutrino production is expected in the standard solar flare model and the properties of these solar flare neutrinos depend on the initial accelerated proton spectrum and flux (Kocharov et al. 1991; Fargion 2004). Measurements of solar flare neutrinos can add an additional probe of these dramatic events and play an important role in the experimental understanding of the particle acceleration on the solar surface.

The Homestake experiment reported a small excess of events correlated with a large solar flare in 1991 (Davis 1994). On the other hand, KAMIOKANDE II and LSD observed no excess of events associated with large solar flares (Hirata et al. 1990; Aglietta et al. 1991). SNO has performed a coincidence search with 842 solar flares taken from the High Energy Solar Spectroscopic Imager (*HESSI*) and found no correlations (Aharmim et al. 2014). However, KAMIOKANDE II, LSD, and SNO have not excluded all of the parameter space which was favored by Homestake. In 2019, an analysis by Borexino of 472 solar flares selected from the *Geostationary Operational Environmental Satellite* (*GOES*) database established 90% C.L. upper limits which excluded the Homestake parameter space (Agostini et al. 2021). The aforementioned studies are sensitive to neutrinos in the 1–100 MeV range. Recently, IceCUBE reported the first search for GeV-scale neutrinos related to intense γ-ray solar flares and constrained some of the parameter space associated with theoretical predictions for the neutrino flux (Abbasi et al. 2021).

* Present address: Imperial College London, Department of Physics, Blackett Laboratory, London SW7 2AZ, UK
† Present address: National Institutes for Quantum and Radiological Science and Technology (QST), Hyogo 679-5148, Japan
‡ Present address: National Research Nuclear University "MEPhI" (Moscow Engineering Physics Institute), Moscow, 115409, Russia
§ Present address: Department of Physics and Astronomy, University of Alabama, Tuscaloosa, AL 35487, USA
¶ Present address: Kamioka Observatory, Institute for Cosmic-Ray Research, The University of Tokyo, Hida, Gifu 506-1205, Japan

In this paper, we present a search for solar flare neutrinos using the KamLAND data taken from 2002 March to 2019 September, which includes Solar cycle 23 and 24. KamLAND is a 1 kton liquid-scintillator anti-neutrino detector which is sensitive to neutrinos in the energy range between 1 MeV and a few GeV. However, in this study we focus on 1–35 MeV neutrinos. We used the *GOES* X-ray data (Hanser & Sellers 1996) to select the flare events and to determine the coincidence time window. We then evaluate the statistical excess of neutrino events in KamLAND in the time window. With the assumption that the fluence of solar flare neutrinos is proportional to the flare X-ray peak flux, the statistics of this search is about 1.7 times larger than previous studies (Agostini et al. 2021); this assumption allows straightforward direct comparison of our result to results from other experiments and theoretical predictions.

2. SOLAR FLARE DATA

In this study, we assume that the solar flare neutrino fluence is proportional to the X-ray intensity at 0.1–0.8 nm. We selected X- and M-class solar flares from the *GOES* X-ray database in Center for Integrated Data Science (CIDAS) at Nagoya University, since the contributions from flares of the other classes are small enough. The time duration of solar flares is typically tens of minutes. In this study, we applied the method described in Okamoto et al. (2020) to determine the flare time window as follows: (i) calculate the differential X-ray light curve, (ii) search for the peak of the differential curves, (iii) define the time window starting from the nearest zero coefficient before the peak and ending at the nearest zero coefficient after the peak (red region in Figure 1).

After the X- and M-class selection, there were 1342 flares with a total X-ray intensity of $639.3 \times 10^{-4}\,\mathrm{W/m^2}$ from 2002 March to 2019 September. For the coincidence analysis with the KamLAND data, all time windows were required to be in a period of operation in which the livetime to running time ratio of the detector was more than 95%. The KamLAND livetime is defined as the integrated period of time that the detector was sensitive to neutrinos and includes corrections for calibration periods, detector maintenance, daily run switch, etc. Applying these requirements, we found 614 solar flares remained. The distributions of the duration and intensity of these flares are shown in Figure 2 and Figure 3, respectively. The average length of the 614 time windows is 1028 s. The integrated intensity is $303.0 \times 10^{-4}\,\mathrm{W/m^2}$, which is 25 times larger than the flare coincident with the Homestake excess and 1.7 times larger than the flares used in the Borexino analysis (Agostini et al. 2021).

3. KAMLAND DETECTOR

The KamLAND detector is a large-volume neutrino detector, which is located approximately 1 km underground under Mt. Ikenoyama in Kamioka, Japan. KamLAND consists of an outer water-Cherenkov detector and an inner scintillation detector. The water-filled outer detector (OD), housed in a 10 m-radius × 20 m-high cylindrical tank, provides shielding from external γ-ray backgrounds and an active muon counter. The OD was instrumented with 225 20-inch Photo Multiplier Tubes (PMTs) before a refurbishment in 2016 and 140 20-inch PMTs after the refurbishment (Ozaki & Shirai 2017). The inner detector is a 9 m-radius stainless steel spherical tank with 1325 17-inch PMTs and 554 20-inch PMTs mounted on the inner surface. The main volume of the inner detector is 1 kton liquid scintillator supported by a 6.5 m-radius nylon/EVOH balloon installed at the center of the stainless steel tank. This nylon/EVOH balloon is called the outer balloon. Outside the outer balloon is filled with non-scintillating buffer oil. Another smaller nylon balloon for KamLAND-Zen is

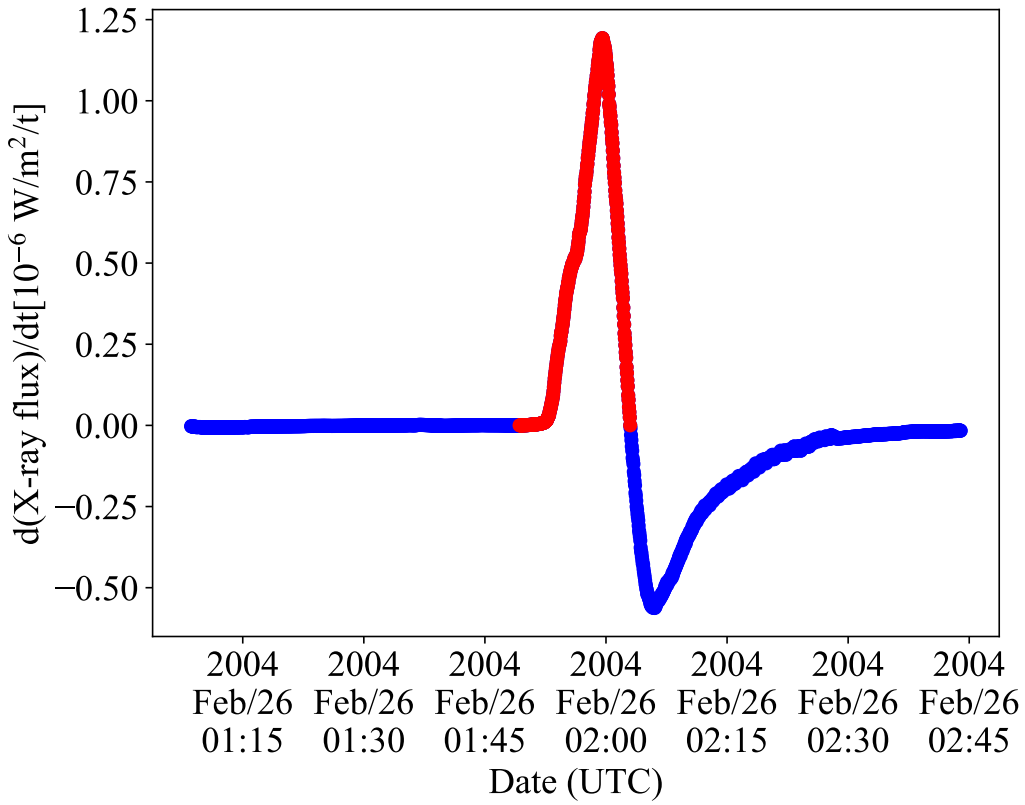

Figure 1. Derivative function of X-ray light curves in a X1.1-class flare on 2004 Feb 26

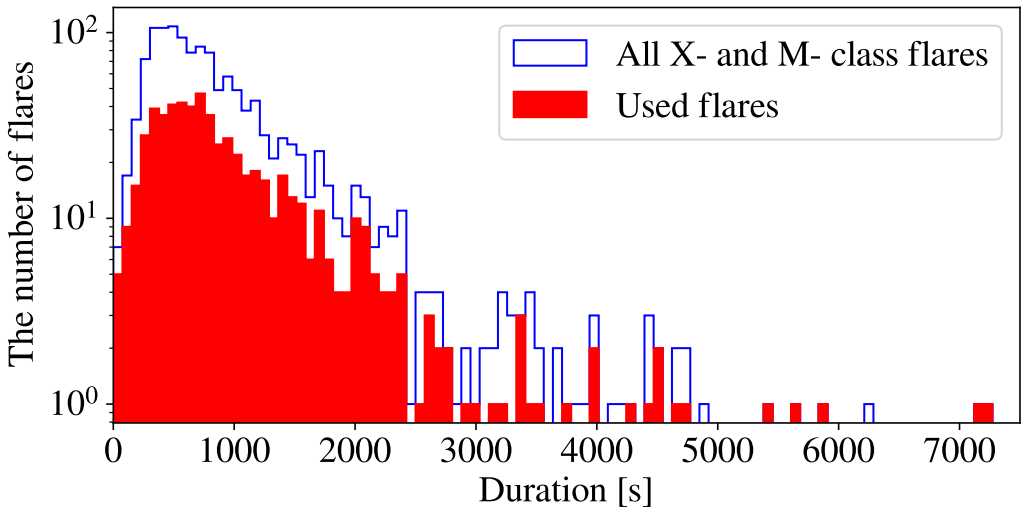

Figure 2. Distribution of the duration time of flares.

called the inner balloon and is described later. The details of the KamLAND detector are described in Suzuki (2014).

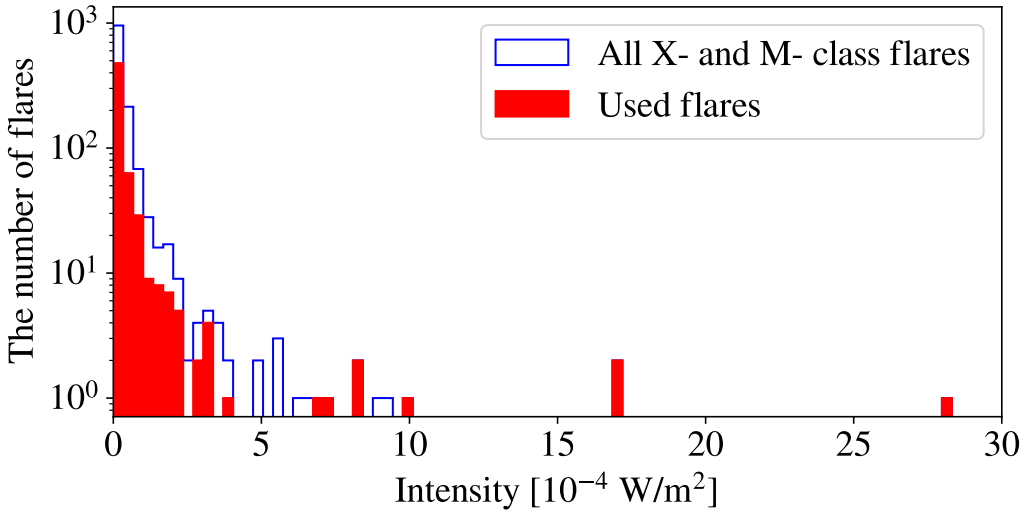

Figure 3. Distribution of X-ray intensity.

KamLAND began data taking in March 2002. From August 2011, KamLAND started the KamLAND-Zen phase to search for the neutrinoless double-beta decay of ^{136}Xe using a nylon balloon (inner balloon) installed at the center of the detector; this inner balloon is filled with xenon-loaded liquid scintillator (Gando et al. 2016). During the initial phase, known as KamLAND-Zen 400, which ran from August 2011 to September 2015, the inner balloon radius was 1.5 m and the mass of xenon was about 400 kg. In 2018 May, the KamLAND-Zen experiment was upgraded to the so-called KamLAND-Zen 800 phase, with an enlarged inner balloon of radius 1.9 m and double the amount of xenon (about 800 kg) for a higher sensitivity search (Gando 2020). For the KamLAND-Zen periods, the regions with xenon-loaded scintillator were excluded from the effective volume for the neutrino search to suppress backgrounds from the xenon nuclei, nylon balloon, and supporting structures.

KamLAND has multiple reaction channels to detect neutrinos. We used the following two channels, neutrino-electron scattering (ES), $\nu + e^- \rightarrow \nu + e^-$, and inverse-beta decay (IBD), $\bar{\nu}_e + p \rightarrow e^+ + n$. ES is sensitive to all flavor of neutrinos, though the cross section depends on the neutrino flavor. This channel does not provide a measurement of the neutrino energy, though the energy of the scattered electron provides a lower bound. IBD is sensitive only to electron anti-neutrinos above 1.8 MeV. The IBD cross section is roughly ten times larger than the ES cross section. In addition, the IBD signal has advantages to suppress backgrounds thanks to a delayed coincidence measurement. The positron annihilates with an electron, emitting two 511 keV γ-rays. The positron and two γ-rays are observed as one event called the prompt event. The incident electron anti-neutrino energy, E_ν, can be reconstructed from the prompt scintillation as $E_\nu \simeq E_p + 0.8\,\mathrm{MeV}$, where E_p is the energy of the prompt signal. With half-live about 207 μs, the neutron captures on a proton (carbon) emitting a 2.2 (4.9) MeV γ-ray, which is called the delayed event. Exploiting time-spatial correlation between the prompt and delayed events, we can observe electron type anti-neutrinos in an almost background free condition.

4. COINCIDENCE ANALYSIS WITH ES

4.1. *Basic treatment of KamLAND data*

Most events in KamLAND are from spallation products and decays of radioactive isotopes on the inner/outer balloons and in the liquid scintillator. Cosmic muons passing through the liquid scintillator generate short-lived isotopes such as ^{8}Li ($\tau = 1.21\,\mathrm{s}$) and ^{12}B ($\tau = 29.1\,\mathrm{ms}$) by spallation on carbon, which is the main component of the liquid scintillator. The muon events and subsequent events which occur within a veto-time window were rejected as muon-spallation related events. The details of the spallation cuts and veto-time definitions are described in Gando et al. (2012a). Cosmic muon spallations also generate long-lived isotopes, ^{10}C. The beta decay of ^{10}C ($\tau = 27.8\,\mathrm{s}$) were rejected by a triple-coincidence tag of a muon, a neutron identified by neutron-capture γ-rays and the ^{10}C decay as described in Gando et al. (2016). Residual decay events from spallation products after the spallation cuts and ^{10}C veto are possible backgrounds for ES events.

To avoid backgrounds from the outer balloon and the spherical stainless-steel tank, events that were detected with $r > 600\,\mathrm{cm}$ are rejected, where r is the distance from the center of the detector. To reject background from the inner balloon and the xenon-loaded liquid scintillator, a 250 cm radius cylinder volume in the upper hemisphere and a $r < 250\,\mathrm{cm}$ volume were rejected only during the KamLAND-Zen 400/800 running periods. One of the serious radioactive isotopes in liquid scintillator is ^{214}Bi in the ^{238}U decay series. Decays of ^{214}Bi to ^{214}Po can contribute background events. Due to the short lifetime of ^{214}Po, these events can be tagged by time-spatial correlation. The details of Bi–Po veto are described in Gando et al. (2012b). Exudation decay events from the Bi–Po veto are another possible backgrounds for ES events.

After applying the vetoes described above, we divided the KamLAND data into 22 periods for ES studies based on the operational status of the detector and the background rate.

4.2. *Selection criteria for ES*

We assume a monochromatic spectrum for the solar flare neutrinos. For each assumed energy, E_ν, an lower energy threshold (E_{th}) and analysis volume ($V(r_{\mathrm{fid}})$) were optimized to maximize the figure of merit (FoM), defined below. In this analysis, we used a spherical analysis volume, thus we optimized the analysis distance, r_{fid}, for the volume, $V(r_{\mathrm{fid}})$. The FoM is defined as

$$\mathrm{FoM} = \frac{V(r_{\mathrm{fid}}) \times P(E_{\mathrm{th}})}{\sqrt{B(r_{\mathrm{fid}}, E_{\mathrm{th}})}}, \tag{1}$$

where $P(E_{\mathrm{th}})$ is the probability that the energy of the ES electron exceeds E_{th}; $B(r_{\mathrm{fid}}, E_{\mathrm{th}})$ is the total number of background events in flare-off time of that period with $r < r_{\mathrm{fid}}$ and $E_{\mathrm{th}} < E_{\mathrm{vis}} < T_{\mathrm{max}}$, where E_{vis} is the observed energy in the KamLAND detector; T_{max} is the maximum kinetic energy of the recoil electron. This optimization was performed period-by-period. The detection efficiency, $\eta^{\mathrm{ES}} = V(r_{\mathrm{fid}})/V(600\,\mathrm{cm}) \times P(E_{\mathrm{th}})$, resulting from the FoM optimization considering the detector energy scale model is shown in Figure 4 as a function of the incident neutrino energy. The shape of $\eta^{\mathrm{ES}}(E_\nu)$ depends on the vertex distribution of external γ-ray backgrounds penetrating the tanks from the rock surrounding the detector.

4.3. *Background estimation and χ^2 studies*

Around $E_\nu = 3\,\mathrm{MeV}$, the background behavior changes. Below 3 MeV, there are large number of backgrounds from radioactive decays in the balloons, PMTs and the inner detector tank, such as

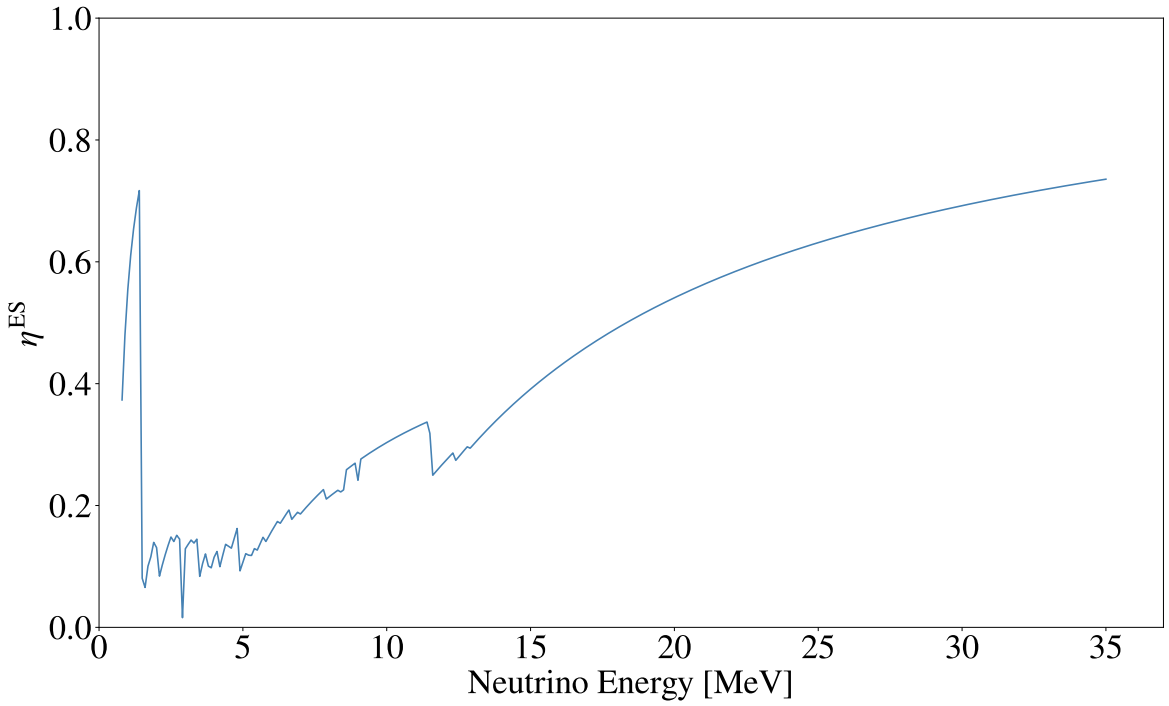

Figure 4. η^{ES} as a function of neutrino energy for one period.

^{208}Tl and ^{40}K. On the other hand, contributions from radioactivity are negligible above 3 MeV. Thus, we estimated the backgrounds above and below 3 MeV separately.

Firstly, we describe the background determination below 3 MeV and flare coincidence analysis. Since the radioactive background rate was not sufficiently stable to estimate the rate in the solar flare time (on-time) due to the liquid scintillator convection in time scale of hours, we estimated the accidental background in the following way. For the i-th flare, 30 off-time windows were opened within a week before the flare. The duration of each off-time window was the same as of the on-time window. In each off-time window, the number of events with $r < r_{\mathrm{fid}}$ and $E_{\mathrm{th}} < E_{\mathrm{vis}} < T_{\mathrm{max}}$ was counted; these are shown as blue dots in Figure 5. We used the average (N_i^{off}) and standard deviation (σ_i) of these off-time samples to estimate the expected number of background events with uncertainty for the associated on-time window. In Figure 5, N_i^{off} and σ_i are shown as a horizontal dashed line and a gray shaded region, respectively. Figure 5 is one example from the M1.8 flare in 2003 with $E_\nu = 1.0$ MeV, where $E_{\mathrm{th}} = 0.4$ MeV and $r_{\mathrm{fid}} = 600$ cm. In this case, N_i^{off} and σ_i are 3567.2 and 80.0, respectively.

The expected number of events in the on-time window with the solar flare signal of the i-th flare is defined as $n_i \equiv N_i^{\mathrm{BG}} + w_i \eta^{\mathrm{ES}} \alpha^{\mathrm{ES}} I_i$; the first term represents the number of background events in the on-time window and the second term corresponds to the number of signal events. The N_i^{BG} are assumed to follow a Gaussian distribution with a mean of N_i^{off} and a standard deviation of σ_i. In the second term, I_i is the flare intensity in units of [10^{-4} W/m^2]; α^{ES} is a scale factor that connects between the flare intensity and the number of ES in the 600 cm-spherical volume, i.e., α^{ES} means how many electron scatterings occur in the 600 cm-spherical volume by a X1 flare; η^{ES} is the detection efficiency described above; w_i is the detector livetime ratio in i-th on-time window. The observed

number of events with $r < r_{\rm fid}$ and $E_{\rm th} < E_{\rm vis} < T_{\rm max}$ in the on-time window for the i-th flare ($N_i^{\rm on}$) should follow a Poisson distribution with a mean of n_i. In the case of Figure 5, $N_i^{\rm on}$ is 3525, and is shown as a red dot.

The χ^2 for all flares can be written as,

$$\chi^2 = 2\sum_{i\in\text{flares}}[N_i^{\rm on} - n_i + n_i\ln(n_i/N_i^{\rm on})] + \sum_{i\in\text{flares}}\left(\frac{N_i^{\rm BG} - N_i^{\rm off}}{\sigma_i}\right)^2. \quad (2)$$

The second term in Equation (2) is a χ^2 penalty to account for the uncertainty on the background rate below 3 MeV, using σ_i as a conservative error. In Equation (2), $\alpha^{\rm ES}$ and $N_i^{\rm BG}$ are free parameters, i.e., this χ^2 was minimized with respect to $\alpha^{\rm ES}$ and $N_i^{\rm BG}$ ($i = 1, 2, \cdots, 613$).

Above 3 MeV, the background rate is small and stable. The mean number of events in the on-time window is $n_i = \langle N_i^{\rm BG}\rangle + w_i\eta^{\rm ES}\alpha^{\rm ES}I_i$, where $\langle N_i^{\rm BG}\rangle$ is the background rate averaged over the period scaled by the coincidence window duration. The χ^2 is modified to

$$\chi^2 = 2\sum_{i\in\text{flares}}[N_i^{\rm on} - n_i + n_i\ln(n_i/N_i^{\rm on})]. \quad (3)$$

This χ^2 was minimized with respect to α.

From the χ^2 scan in our analysis range of 0.4–35 MeV for E_ν, the best-fit $\alpha^{\rm ES}$, $\alpha^{\rm ES}_{\rm best}$, was 0 for all assumed neutrino energies. The 90% confidence level (C.L.) upper limit on $\alpha^{\rm ES}$, $\alpha^{\rm ES}_{90}$, was estimated from $\chi^2(\alpha^{\rm ES}_{\rm best}) + 2.7 = \chi^2(\alpha^{\rm ES}_{90})$. The 90% confidence interval of $\alpha^{\rm ES}$ is shown as a function of the assumed neutrino energy in Figure 6.

5. COINCIDENCE ANALYSIS WITH IBD

5.1. *Selection criteria for IBD*

After the basic vetoes described in Section 4.1, the data were divided into 12 periods. The definition of the periods are not the same as the ES analysis since the background conditions for IBD are quite different because of the time-spatial correlation selection.

The prompt events were selected by requiring the reconstructed energy to be between 0.9–35 MeV with the delayed signal on a proton (^{12}C) between 1.8–2.6 MeV (4.4–5.6 MeV). The prompt-delayed pair was defined by requiring that the vertices of the two signals were less than 200 cm apart and the time of the delayed signal must be within 0.5–1000 μs of the prompt signal. Additionally, a likelihood-based signal selection was applied to improve the purity of the IBD candidates against accidental coincidence backgrounds.

The standard IBD candidate selection used in KamLAND, and in this analysis, is summarized in Asakura et al. (2015).

5.2. *Background estimation and χ^2 studies*

The IBD event rate is low and stable within each period because of the strong background reduction with the time-spatial correlation. Thus, a different χ^2 is defined as

$$\chi^2 = 2\sum_{p\in\text{period}}[N_p^{\rm on} - n_p + n_p\ln(n_p/N_p^{\rm on})], \quad (4)$$

where $n_p = \langle N_p^{\rm off}\rangle + w_p\eta^{\rm IBD}\alpha^{\rm IBD}I_p$ is the expected number of events in the cumulative flare time window, i.e., summed over all coincidence windows for the flares in our sample in the p-th period.

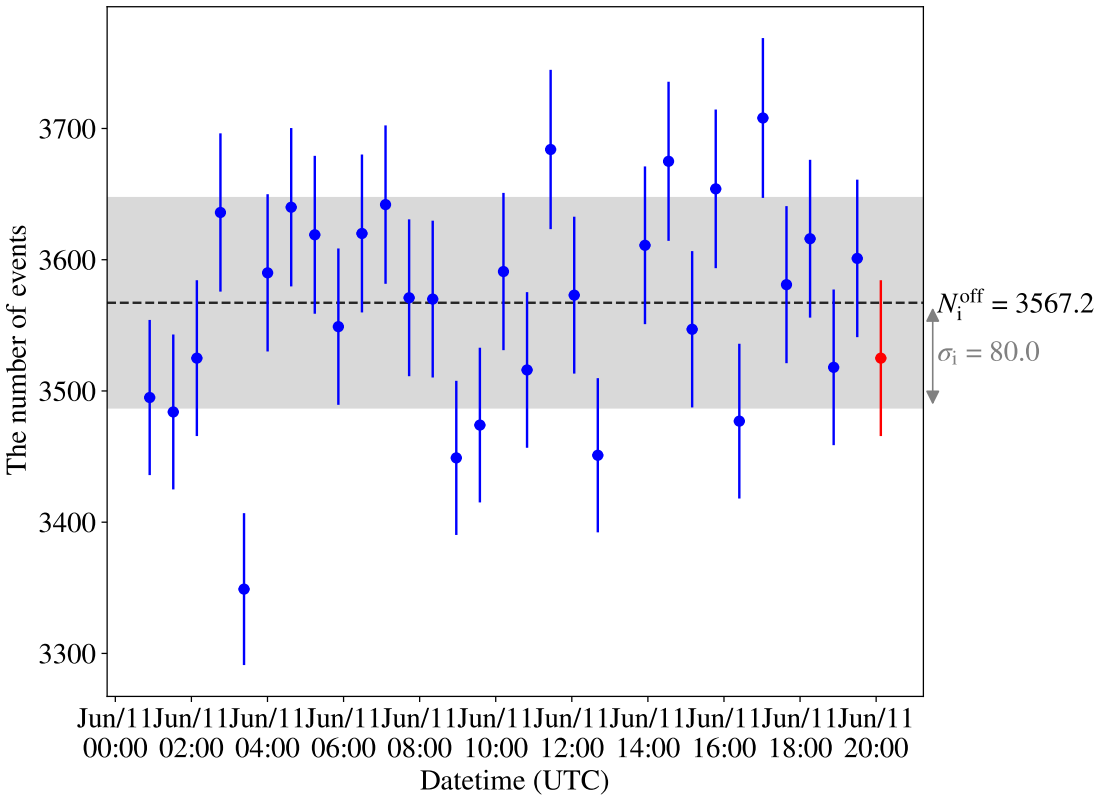

Figure 5. Example of $N_i^{\rm on}$, $N_i^{\rm off}$ and σ_i as defined in the text. The red point is the number of observed events, $N_i^{\rm on}$, in the flare time window. The thirty blue points show the event rate in each of the off-time windows scaled by the detector livetime in that window. The horizontal dashed black line shows $N_i^{\rm off}$. The horizontal gray band shows the region $[N_i^{\rm off} - \sigma_i,\ N_i^{\rm off} + \sigma_i]$, In this example, the flare is the M1.8 flare in 2003. Assumed neutrino energy is 1.0 MeV. $N_i^{\rm off}$ and σ_i are 3567.2 and 80.0, respectively.

The $N_p^{\rm off}$ is the expected no-flare contribution, which is estimated from the IBD event rate in the p-th period excluding the flare time window and scaled to the duration of the flare time window. $N_p^{\rm on}$ is the number of IBD events observed in the cumulative flare time window in the p-th period. I_p is the cumulative X-ray intensity in the p-th period. The parameter $\alpha^{\rm IBD}$ is a scale factor that connects between flare intensity and the number of IBD in the 600 cm-spherical volume. In the IBD analysis, we used $r_{\rm fid} = 600$ cm as the analysis distance and no energy binning to count events for the χ^2 study. The $\eta^{\rm IBD}$ indicates the detection efficiency for the electron anti-neutrinos via IBD, and is computed with Monte Carlo simulation as shown in Figure 7. In the region below 4 MeV, the efficiencies are reduced due to larger accidental backgrounds which affect the likelihood selection. Because of the inner-balloon volume cuts during the KamLAND-Zen 400/800 phases as described in Section 3, the efficiencies in some periods are lower than in other periods. Above about 4 MeV, the efficiencies converge to ∼77% for the inner-balloon cut periods and ∼94% for other periods. w_p is the detector livetime ratio.

Assuming a monochromatic spectrum for the solar flare neutrinos, we varied E_ν from 1.8 MeV to 35 MeV, and found $\alpha^{\rm IBD}$ which minimize χ^2 for each assumed neutrino energies. The best-fit values of $\alpha^{\rm IBD}$, $\alpha^{\rm IBD}_{\rm best}$, and the 90% C.L. upper limits on $\alpha^{\rm IBD}$, $\alpha^{\rm IBD}_{90}$, were estimated with the same method

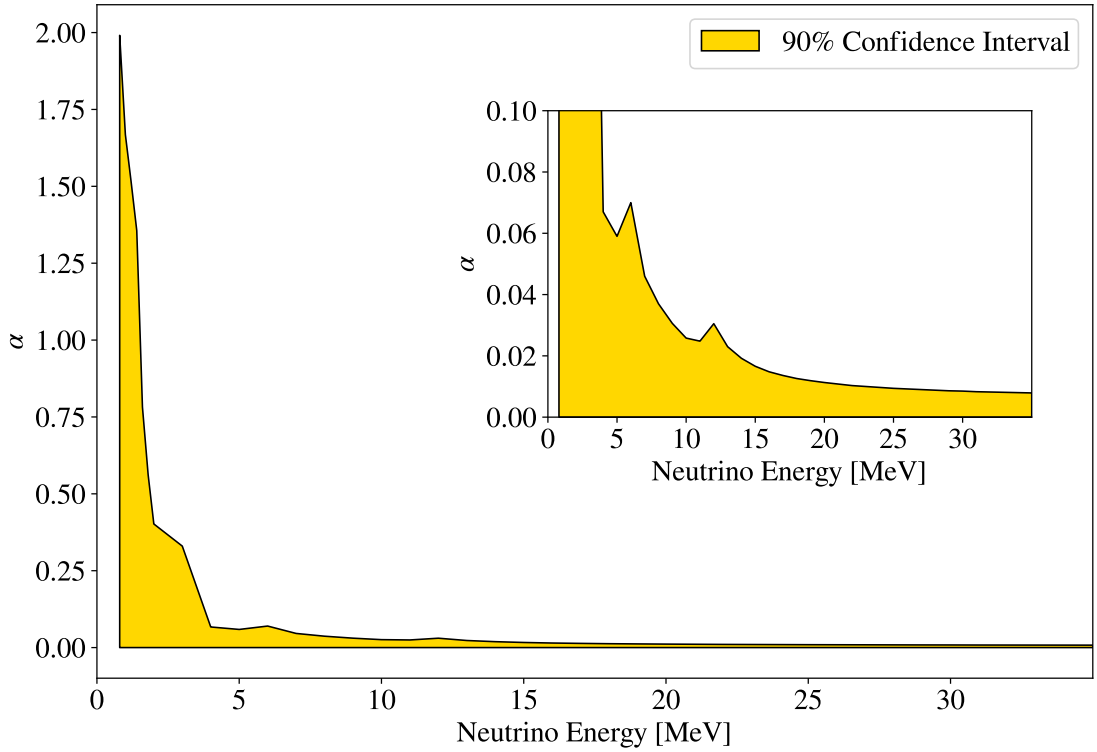

Figure 6. The 90% confidence interval of $\alpha^{\rm ES}$ as a function of neutrino energy in the ES analysis. The inset panel shows the same plot in a different vertical scale.

in the ES analysis. The $\alpha^{\rm IBD}_{\rm best}$ was 0 for all assumed neutrino energies. The 90% confidence interval of $\alpha^{\rm IBD}$ is shown in Figure 8.

6. FLUENCE UPPER LIMIT

Although there are some theoretical predictions of the spectrum of solar flare neutrinos (Kocharov et al. 1991; Fargion 2004), it has not been experimentally measured. Keeping the assumption of the monochromatic signal, we converted $\alpha^{\rm ES}_{90}$ into an upper limit on neutrino fluence, $\Phi^{\rm ES}(E_\nu)$, as

$$\Phi^{\rm ES}(E_\nu) = \frac{\alpha^{\rm ES}_{90}(E_\nu)}{N_e \int_0^{T_{\rm max}} \sigma(E_\nu, E_e) dE_e}, \tag{5}$$

for the ES studies, where N_e is the number of electrons in the 6 m-radius spherical volume: 2.4×10^{32}, E_e is the kinetic energy of recoil electron, $\sigma(E_\nu, E_e)$ is the cross section of electron scattering with the incident neutrino of energy E_ν, and $T_{\rm max}$ is the maximum E_e. For the IBD studies, the upper limit on neutrino fluence, $\Phi^{\rm IBD}(E_\nu)$, was obtained from

$$\Phi^{\rm IBD}(E_\nu) = \frac{\alpha^{\rm IBD}_{90}(E_\nu)}{N_p \sigma(E_\nu)}, \tag{6}$$

where N_p is the number of protons in the 6 m-radius spherical volume: $(5.98 \pm 0.13) \times 10^{31}$, $\sigma(E_\nu)$ is the total cross section of IBD from Strumia & Vissani (2003).

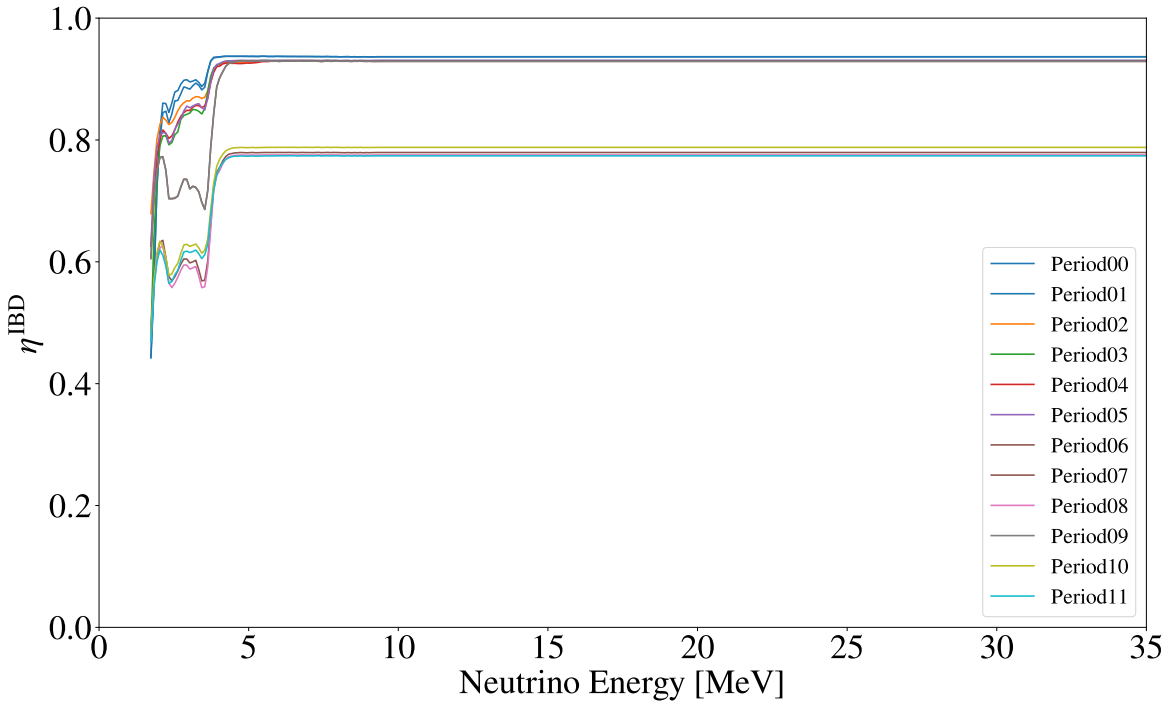

Figure 7. η^{IBD} as a function of neutrino energy for each periods

The fluence upper limits were scaled to the Homestake flare's intensity (X12) as

$$\Phi(E_\nu)^{\mathrm{scaled,ES/IBD}} = \Phi^{\mathrm{ES/IBD}}(E_\nu)\frac{12\times10^{-4}\,\mathrm{W/m^2}}{303.3\times10^{-4}\,\mathrm{W/m^2}}, \tag{7}$$

and shown in Figure 9. The last term in Equation (7) represents the scaling factor from the flares analyzed in this work to the Homestake flare. The allowed fluence region from the Homestake's excess (Aharmim et al. 2014) is shown in the purple band. The upper limit by Borexino (Agostini et al. 2021) is shown as green curves after scaling to the X12 flare. Here, it is difficult to directly compare the results from KAMIOKANDE II (Hirata et al. 1990) and SNO (Aharmim et al. 2014) because of the lack of X-ray measurements for the corresponding flares.

The 90% C.L. upper limits from this work exclude the entire region of parameter space associated with the Homestake event excess for the large solar falre in 1991.

7. SUMMARY

We observed no evidence for neutrinos associated with solar flares in KamLAND. This work placed the most stringent upper limits on fluence normalized to the X12 flare with the assumption that neutrino fluence is proportional to the X-ray intensity. At 20 MeV, the obtained 90% C.L limits are $8.4\times10^{7}\,\mathrm{cm^{-2}}$ for electron anti-neutrinos and $3.0\times10^{9}\,\mathrm{cm^{-2}}$ for electron neutrinos. The Homestake region is independently rejected by this result. To our knowledge, this is the first time to present the upper limit normalized to the flare intensity. We believe that this approach is useful to compare to results from other experiments and theoretical predictions.

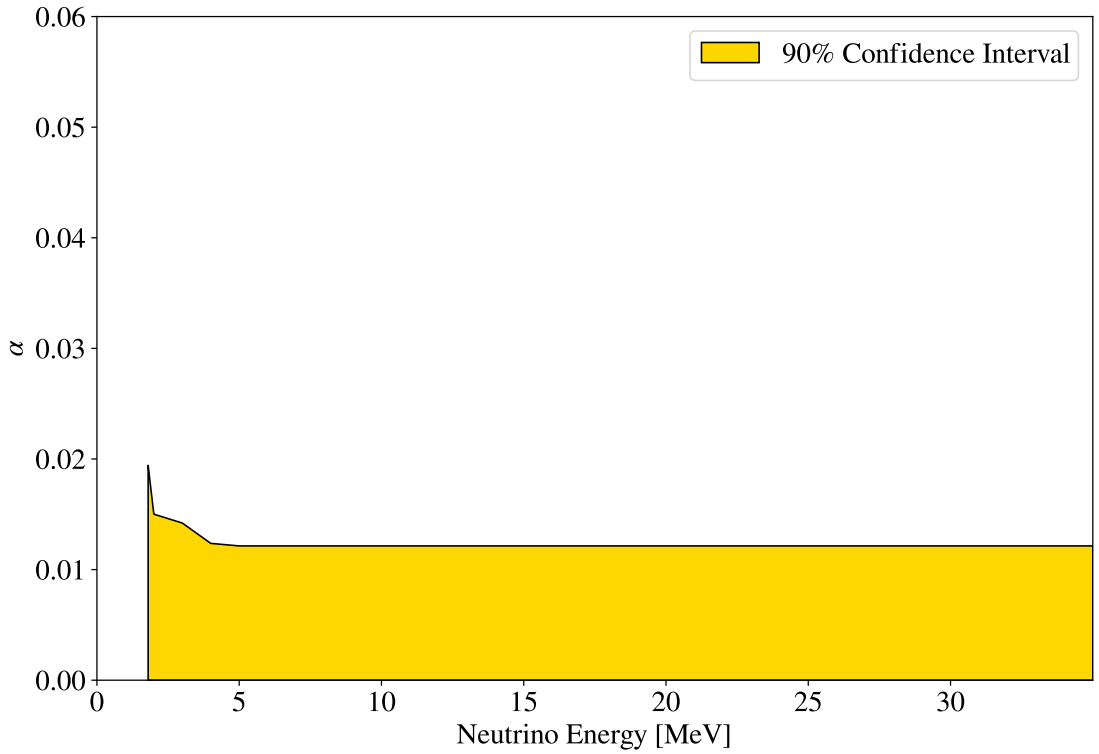

Figure 8. The 90% confidence interval of α^{IBD} as a function of neutrino energy in the IBD analysis.

ACKNOWLEDGMENTS

The KamLAND experiment is supported by JSPS KAKENHI Grants 19H05803; the World Premier International Research Center Initiative (WPI Initiative), MEXT, Japan; Netherlands Organization for Scientific Research (NWO); and under the U.S. Department of Energy (DOE) Contract No. DE-AC02-05CH11231, the National Science Foundation (NSF) No. NSF-1806440, NSF-2012964, as well as other DOE and NSF grants to individual institutions. The Kamioka Mining and Smelting Company has provided services for activities in the mine. We acknowledge the support of NII for SINET4. This work is partly supported by the Graduate Program on Physics for the Universe (GP-PU), and the Frontier Research Institute for Interdisciplinary Sciences, Tohoku University. A part of this study was carried out by using the computational resources of the Center for Integrated Data Science, Institute for Space-Earth Environmental Research, Nagoya University through the joint research program.

REFERENCES

Abbasi, R., et al. 2021, PhRvD. https://journals.aps.org/prd/accepted/be07dQb1N111ad21462f4de02846f4551314f9604

Aglietta, M., et al. 1991, ApJ, 382, 344, doi: 10.1086/170722

Agostini, M., Altenmüller, K., Appel, S., et al. 2021, APh, 125, 102509, doi: https://doi.org/10.1016/j.astropartphys.2020.102509

Aharmim, B., Ahmed, S., Anthony, A., et al. 2014, APh, 55, 1–7, doi: 10.1016/j.astropartphys.2013.12.004

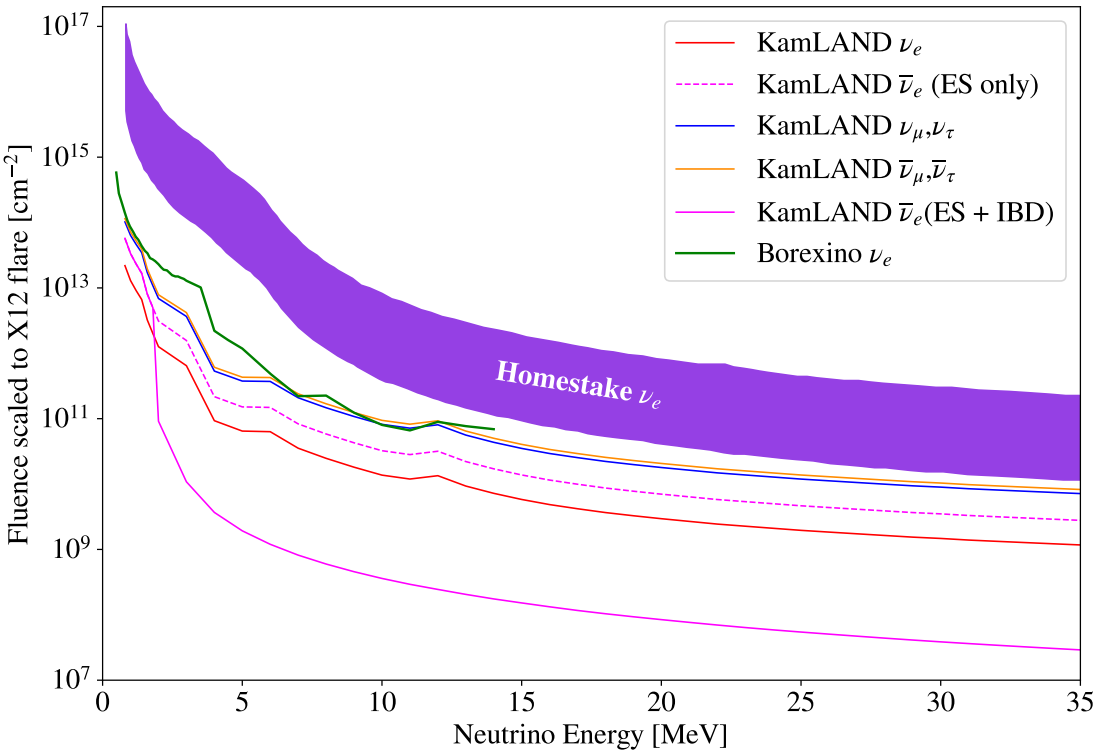

Figure 9. Fluence upper limit scaled to the Homestake flare intensity

Asakura, K., Gando, A., Gando, Y., et al. 2015, ApJ, 806, 87, doi: 10.1088/0004-637x/806/1/87

Benz, A. O. 2008, LRSP, 5, 1, doi: 10.12942/lrsp-2008-1

Davis, R. 1994, PrPNP, 32, 13 , doi: 10.1016/0146-6410(94)90004-3

Fargion, D. 2004, JHEP, 2004, 045, doi: 10.1088/1126-6708/2004/06/045

Gando, A., Gando, Y., Ichimura, K., et al. 2012a, ApJ, 745, 193, doi: 10.1088/0004-637x/745/2/193

Gando, A., Gando, Y., Hanakago, H., et al. 2012b, PhRvC, 85, 045504, doi: 10.1103/PhysRevC.85.045504

Gando, A., Gando, Y., Hachiya, T., et al. 2016, PhRvL, 117, 082503, doi: 10.1103/PhysRevLett.117.082503

Gando, Y. 2020, Journal of Physics: Conference Series, 1468, 012142, doi: 10.1088/1742-6596/1468/1/012142

Hanser, F. A., & Sellers, F. B. 1996, in GOES-8 and Beyond, ed. E. R. Washwell, Vol. 2812, International Society for Optics and Photonics (SPIE), 344 – 352, doi: 10.1117/12.254082

Hirata, K., Kajita, T., Kifune, T., et al. 1990, ApJ, 359, 574, doi: 10.1086/169088

Kocharov, G. E., Kovaltsov, G. A., & Usoskin, I. G. 1991, Il Nuovo Cimento C, 14, 417, doi: 10.1007/BF02509184

Okamoto, K., Nakano, Y., Masuda, S., et al. 2020, SoPh, 295, 133, doi: 10.1007/s11207-020-01706-z

Ozaki, H., & Shirai, J. 2017, PoS, ICHEP2016, 1161, doi: 10.22323/1.282.1161

Schrijver, C. J., et al. 2012, JGR, 117, A08103, doi: 10.1029/2012JA017706

Shibata, K. 1998, Ap&SS, 264, 144, doi: 10.1023/A:1002413214356

Strumia, A., & Vissani, F. 2003, PhLB, 564, 42–54, doi: 10.1016/s0370-2693(03)00616-6

Suzuki, A. 2014, EPJC, 74, 3094, doi: 10.1140/epjc/s10052-014-3094-x